Engineered Nanorod Perovskite Film Photocatalysts to Harvest Visible Light

ARTICLE *in* ADVANCED MATERIALS · MAY 2011

Impact Factor: 17.49 · DOI: 10.1002/adma.201004171 · Source: PubMed

6 AUTHORS, INCLUDING:

Pramod Borse
International Advanced Research Centre fo…
95 PUBLICATIONS **1,651** CITATIONS
SEE PROFILE

Chang Won Ahn
University of Ulsan
133 PUBLICATIONS **1,237** CITATIONS
SEE PROFILE

Euh Duck Jeong
Korea Basic Science Institute KBSI
167 PUBLICATIONS **1,004** CITATIONS
SEE PROFILE

Jason JS Lee
National Yang Ming University
612 PUBLICATIONS **13,167** CITATIONS
SEE PROFILE

Engineered Nanorod Perovskite Film Photocatalysts to Harvest Visible Light

Hyun Gyu Kim, Pramod H. Borse, Jum Suk Jang, Chang Won Ahn, Euh Duck Jeong, and Jae Sung Lee**

The recent flourishing of nanostructured materials has widened its potential applications in the much-desired efficient energy materials. Specifically, materials for solar hydrogen production by water splitting should possess superior optoelectric properties in addition to suitable band energetics and durability in aqueous solutions. The tunability of the physicochemical properties of nanostructred materials by virtue of their size and shape renders a wider applicability. Since the critical limitation of popular TiO_2 photocatalyst that absorbs only UV light,[1,2] the field of visible light water splitting photocatalyst is currently being nurtured by various kinds of conventional and new single component materials (CdS, WO_3, Fe_2O_3, TaON, etc.), as well as composite materials.[3–20] However, there is still much potential for nanostructured materials in this area. There have been several reports on the binary[3–6] and ternary metal oxides,[7–13] composite metal oxides, and modified nanocomposites[14–20] to tackle the problem of efficiency and stability improvement. To this end, the special emphasis has been given to exploring and improving their electronic, structural, and chemical properties by nanostructuring these materials.

In the present report, we attempt to use an Aurivillius phase perovskite $PbBi_2Nb_2O_9$ (PBNO) photocatalyst in its nanorod configuration for the fabrication of photoelectrode for a photoelectrochemical (PEC) water splitting. The PBNO was shown to be an efficient and stable photocatalyst for visible light water splitting, as well as for the photodegradation of organic pollutants in particulate reaction systems.[15] Yet, it has not been utilized in PEC cell applications due to its complex material processing conditions and requirements for the film fabrication. In order to utilize PBNO as a PEC electrode material, it is required to deposit the PBNO layer over a transparent conducting oxide (TCO) substrate (e.g., F doped tin oxide (FTO)). In general, a TCO displays a drift and irreversible changes in the electrical properties above 500 °C and perovskite structures, especially containing more than two metal atoms in the crystal lattice, require a high temperature (>1200 °C) and a long thermal treatment (>50 h) to acquire the thermodynamically stable phase. Hence it is difficult to achieve the desired PBNO phase under the fabrication conditions without altering the electrical properties of TCO. In addition, we attempt to fabricate the oriented 1D nanostructure film on TCO to optimize the performance of PBNO. It is known that 1D nanostructures offer superior optoelectrical properties relative to random particles.[21]

We have successfully fabricated a PBNO nanorods (denoted as PBNO-NR) film as a photoelectrode for the PEC cell. Further we have also shown for the first time that, relative to particle film, the PBNO-NR configuration dramatically improves the performance of photocurrent generation during PEC electrolysis of water under visible light irradiation.

Detailed procedures are described in the Supporting Information for the fabrication of a novel nanorod PBNO photoelectrode for PEC water oxidation. As shown schematically in **Figure 1**A, fabrication of photoelectrode involves the use of homemade anodic aluminum oxide (AAO) as a template for the formation of PBNO-NR. The PBNO sol is spin-coated over the AAO template to infiltrate the alumina pores and later convert to PBNO-NR. Accordingly, upon infiltration, the assembly of sol-AAO is subjected to annealing around 960 °C for crystallization of PBNO-NR. Further, the sintered assembly of PBNO in AAO columnar pores is pressed over a Ag-coated FTO substrate and further annealed around 150 °C to acquire a better adhesion between nanorods formed inside AAO and the Ag-coated FTO. The separate high-temperature synthesis of PBNO-NR followed by its transfer to FTO is a critical step to acquire highly crystalline nanorods without degrading the FTO. The next step was to extract the PBNO-NR by etching out the AAO template. The obtained PBNO-NR attached to FTO was given a treatment with Ag-sol over the external surface of nanorod array. Figure SI.1 (Supporting Information) shows a transmission electron microscopy (TEM) image that reveals Ag particles dispersed on PBNO-NR. Figure 1B–D depict the morphological and elemental evolution during the fabrication of the PBNO-NR electrode. A high-denisty, vertically aligned array of nanorods showed uniform shape and size (0.2 μm in diameter and 6 μm in length). Figure 1C,D show the elemental compositions analyzed by energy dispersive spectrometry (EDS). The formed Ag-coated PBNO-NR/Ag/FTO electrode was used as the PEC photoanode.

For direct comparison of the PEC properties between nanorods and particles, PBNO powder made by a solid-state reaction (SSR) was separately used for the fabrication of the photoanode. **Figure 2** displays schematic procedures and the morphology of a photoelectrode made of the SSR powder (denoted as PBNO-SSR) that was used as reference in this work. As

Dr. H. G. Kim, Dr. C. W. Ahn, Dr. E. D. Jeong
Korea Basic Science Institute
Busan center, Busan 609-735, Korea
E-mail: hhgkim@knbsi.re.kr
Dr. J. S. Jang, Prof. J. S. Lee
Department of Chemical Engineering/Division of Advanced Nuclear Engineering
Pohang University of Science and Technology (POSTECH)
San 31 Hyoja-dong, Pohang, 790–784, Korea
E-mail: jlee@postech.ac.kr
Dr. P. H. Borse
Interanational Advanced Center for Powder Metallurgy & New Materials
Hyderabad, AP 500005, India

DOI: 10.1002/adma.201004171

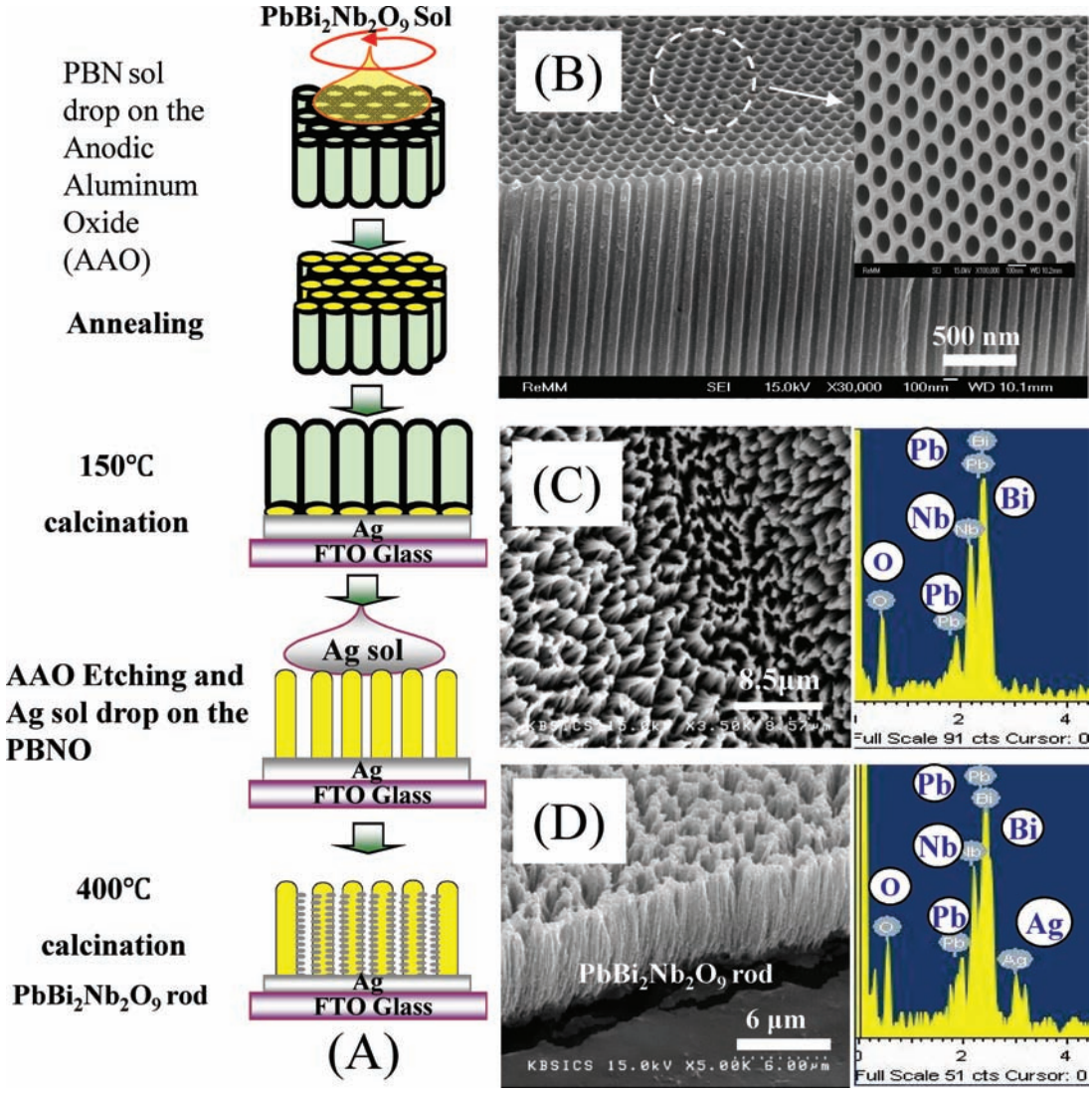

Figure 1. A) Schematic illustration of the technique adopted for the synthesis of PBNO nanorods by an AAO template method and deposition of the PBNO nanorods on the FTO substrate. B) Typical field-emission scanning electron microscopy (FESEM) image of the cross-section of the AAO template with a top view in the inset. C) Surface of PBNO nanorods in AAO before etching with elemental analysis by EDS. D) Cross-sectional view of PBNO nanorods after applying Ag-sol over the film on the FTO substrate and EDS elemental analysis.

shown in Figure 2A, the PBNO-SSR particles were used for screen printing over the Ag-coated FTO. To obtain the film, the screen-printed coating was subjected to calcination (to remove poly(ethylene glycol) (PEG), which was used as a binder) after drying. Ag particles were dispersed over the PBNO layers. This was done by spin-coating $AgNO_3$ sol over the PBNO surface followed by calcination. The final fabricated electrode is shown in Figure 2B. The morphology of the film surface and the particle morphology are shown in Figure 2C in the scanning electron microscopy (SEM) images. The cross-sectional schematic of the fabricated PBNO-SSR/Ag/FTO film electrode is shown in Figure 2D and displays the randomly oriented particles over the film surface. This is in contrast to the photoelectrode fabricated by using PBNO-NR, which shows a uniform, vertically aligned nanorod array.

The results of structural characterization of the films PBNO-NR and PBNO-SSR are shown in **Figure 3**. Both films exhibit an Aurivillius phase of $PbBi_2Nb_2O_9$ (orthorhombic) structure. The oriented nanorod film additionally shows the substrate (FTO) peaks, which are not observed in the powder-coated film, due to existence of a thick film. The respective insets clearly reveal the morphological differences in the film constituents. The corresponding TEM and high-resolution TEM (HRTEM) images (shown in the inset) clearly reveal the fringes of the layered structure. This demonstrates that the highly crystalline PBNO phase exists in the particles as well as in the nanorod constituents of the photoelectrode.

Results of the PEC performance are shown in **Figure 4**A for the nanorod and powder films under visible light irradiation (>420 nm). It is clear that both of the PBNO films show PEC activity, but nanorod photoanodes show dramatically higher performance than the particulate (SSR) electrodes. The PBNO-NR and Ag-modified PBNO-NR photoanodes display 10 and 20 times higher photocurrents than the PBNO-SSR photoanode.

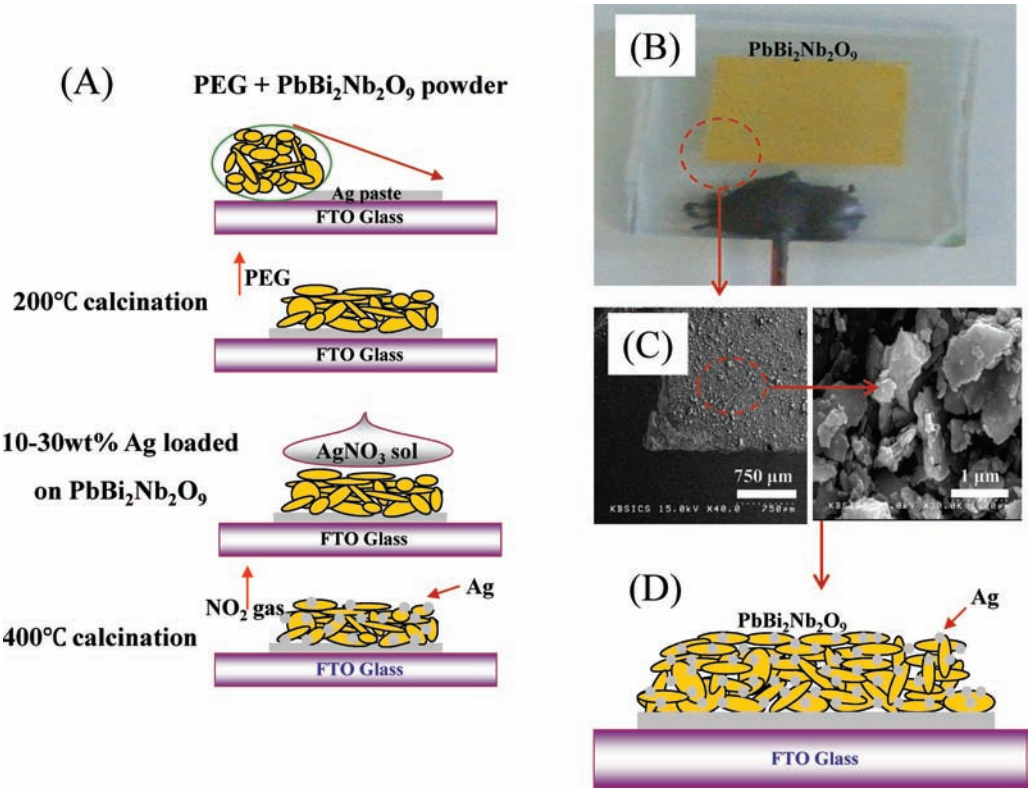

Figure 2. A) Schematic illustration of the process adopted for the deposition of the PBNO-SSR powder on the FTO substrate. B) The fabricated PBNO powder (SSR) photoelectrode on FTO deposited by screen printing with a film surface and particle morphology. SEM image is shown in (C). D) Cross-sectional schematic of screen printed powder (SSR) film on Ag-coated FTO substrate.

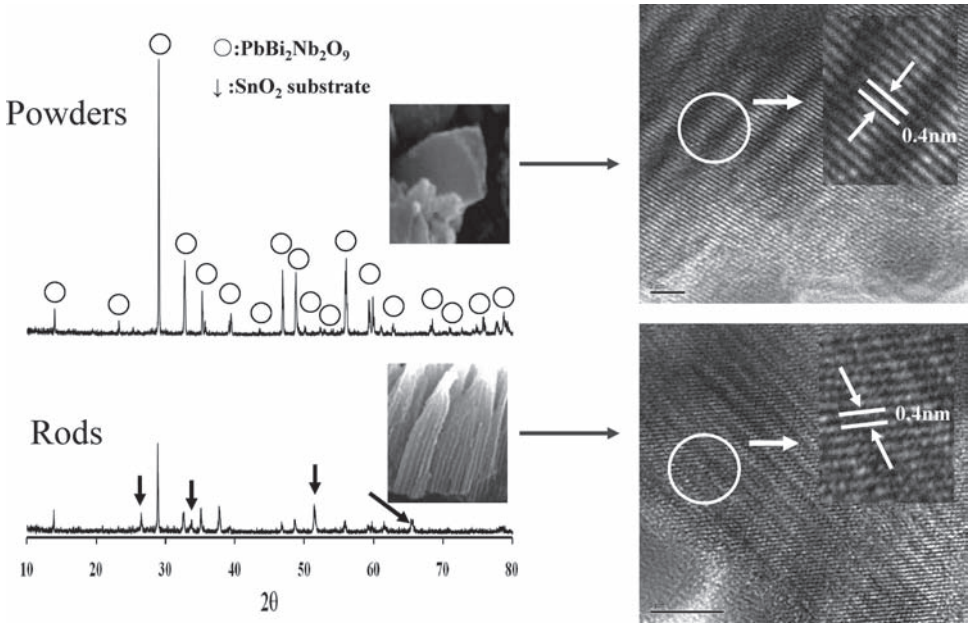

Figure 3. X-ray diffraction patterns of the PBNO-SSR (top) and PBNO-NR (bottom) films. Their insets show the FESEM images of the respective film surface. The right-hand panels show the TEM and HRTEM (insets) images of the scratched particles transferred to a Cu grid.

These electrode/electrolyte systems show the onset potential in the range of –0.2 V to –0.4 V versus a Ag/AgCl reference potential in the following order: Ag-PBNO-NR < PbNO-NR < PBNO-SSR. The observed difference in the onset can be attributed to the change in morphology from a particle to a rod structure and a possible effect of Ag-modification. Figure 4B shows

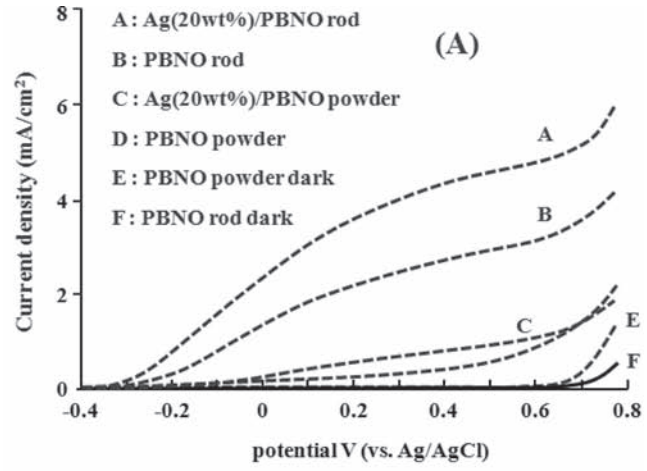

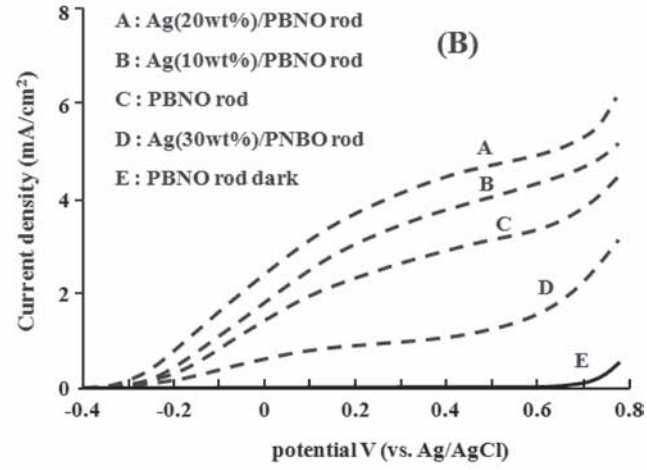

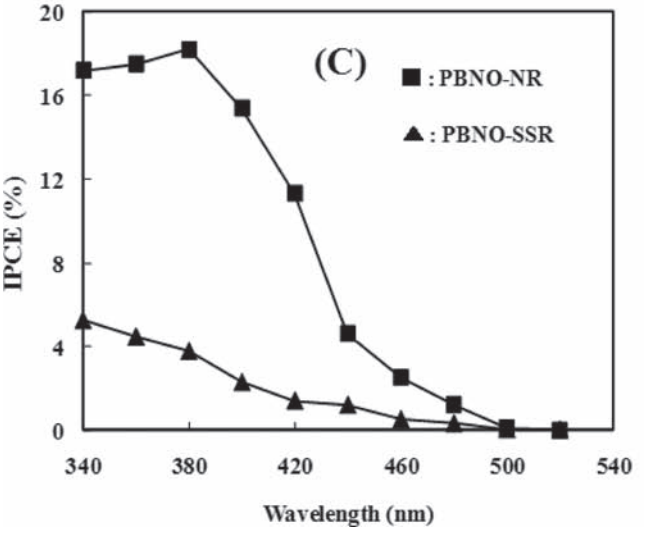

Figure 4. Photocurrent density potential curves of photoelectrode of A) PBNO-SSR/FTO, PBNO-NR/FTO, and Ag/PBNO-NR/FTO and B) PBNO-NR with variation in the Ag component in the photoanode film vs a Ag/AgCl electrode. The electrode was illuminated using a 420 nm optical filter with a 300 watt Xe source. Electrolyte: 0.1 M NaOH (pH = 12.3); scan rate: 100 mV s^{-1}; illuminated photoanode area: 1.0 cm^2 in all cases. C) IPCEs recorded in 0.1 M NaOH for rods and powder photoanodes.

the effect of Ag concentration on the Ag-modified PBNO-NR photoanode. As observed, the photoanodes with Ag concentrations of 10, 20, and 30 wt% are compared with the unmodified (i.e., PBNO-NR) electrode. The Ag (30 wt%) PBNO-NR sample showed a reduced photocurrent compared to the unmodified one, whereas 10 wt% and 20 wt% showed increased photocurrents. The Ag (20 wt%) PBNO-NR showed a maximum photocurrent, indicating that 20 wt% is the optimum concentration for the generating high photocurrents. A high current density of 2.42 mA cm^{-2} was observed even without an applied voltage. The positive role of Ag is attributed to the catalytic effect on the anodic reaction and enhanced electron transfer at the electrode/electrolyte interface. However, an excessive amount of Ag causes a negative effect, probably because it blocks the active PBNO sites. Further, the incident photon conversion efficiency (IPCE) was estimated by measuring the photocurrent generated from photoanodes of Ag (20 wt%), PBNO-NR, and PBNO-SSR (Figure 4C). The measurements demonstrate that the nanorod photoanode is ca. 2–4 times more efficient than the particle photoanode in the wavelength range of 450–340 nm.

To confirm that the currents generated from the photoelectrochemical reaction are indeed from water splitting reactions, the gas phase of the reactor was analyzed under the chronoamperometry conditions using a sealed two-electrode cell with photoelectrode (working electrode) and a platinum foil (counter electrodes) under no bias. According to a band diagram (Figure SI.2,3, Supporting Information) determined by measuring the flat band potential, $PbBi_2Nb_2O_9$ has the right potential for generation of hydrogen and oxygen from water. The results of gas evolution are presented in Figure SI.4 (Supporting Information) for Ag (20 wt%) PBNO-NR and PBNO-SSR. Significant amounts of gases were produced only from Ag (20 wt%) PBNO-NR in agreement with Figure 4 and the H_2:O_2 mole ratio was 2:1 as expected. Thus it has been demonstrated that the currents observed in Figure 4 are due to water splitting reaction.

Thus in the present work, Aurivillius phase perovskite PBNO photocatalyst has been demonstrated to become a highly efficient electrode material for PEC applications, particularly when it is in its nanorod configuration. To elucidate the difference in the mechanism of charge transport in particle and nanorod photoanodes, illustrations are shown in **Figure 5**. When a photoanode of PEC cell is illuminated, the light-induced electron–hole pairs result in splitting of water (H_2O) molecules into gaseous oxygen (O_2), hydrogen ions (H^+), and electrons.

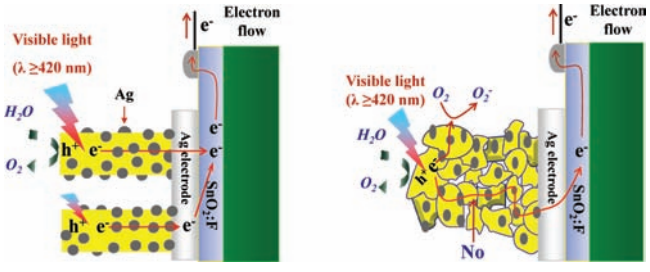

Figure 5. Schematic model displaying the illuminated photoanode, explaining the charge transport in A) PBNO-NR and B) PBNO-SSR photoanode film of a PEC cell.

The process takes place at the photoanode/electrolyte interface and, consequently, oxygen gas is evolved at the photoanode and H^+-ions migrate to the cathode through the electrolyte. Simultaneously, the generated photoelectrons move to the external circuit to reach the cathode, resulting in reduction of the H^+ ions at the cathode where the hydrogen gas is evolved. The efficiency of the photoanode depends on several parameters, mainly the electron–hole recombination rate. The rate, in turn, depends mainly on the charge transport properties in the electrolyte/photoanode/back electrode configuration. Here, the directional electron transport in crystalline PBNO nanorods in Figure 5A is expected to be several orders of magnitude faster than the percolation through a random polycrystalline PBNO network in Figure 5B.[21] The electron migration between the interfaces is greatly affected by the large number of interfaces in particles as compared to the nanorods that favors the charge transport along a rod axis. This kind of axial charge transport path in nanorods reduces the chance of recombination during the migration of electron from the photoanode to the back electrode and enhances the efficiency of the PBNO-NR photoanode.

Experimental Section

Detailed experimental procedures are described in the Supporting Information. For preparation of the PBNO precursor solutions, lead acetate trihydrate ($Pb(C_2H_3O_2)_2{\cdot}3H_2O$, Aldrich, 99.99%), bismuth nitrate pentahydrate ($Bi(NO_3)_3{\cdot}5H_2O$, Sigma-Aldrich 99.99%), and niobium pentaethoxide ($Nb(OC_2H_5)_5$, Aldrich 99.95%) were used as the starting material. 2-Methoxy ethanol ($C_3H_8O_2$, Sigma-Aldrichi 99.8%) and acetylacetone ($C_5H_8O_2$, Sigma-Aldrich 99%) were used as the solvent and chelating agent, respectively. To compensate for the loss of Pb during thermal annealing, 10 mol% excess of the Pb precursor was added to the PBNO precursor solutions. The concentration of PBNO in the final solution was adjusted to a value of ≈0.4 mol L^{-1}. The fabrication of photoelectrode involves use of homemade anodic aluminum oxide (AAO) as a template for the formation of PBNO-NRs. The PBNO sol was spin-coated over the AAO template to infiltrate the alumina pores and was later converted to PBNO-NR. Accordingly, upon infiltration, the assembly of sol-AAO was subjected to annealing around 960 °C for crystallization of PBNO-NR. Further, the sintered assembly of PBNO in AAO columnar pores was pressed over a Ag-coated FTO substrate and further annealed around 150 °C to acquire a better adhesion between nanorods formed inside AAO and the Ag-coated FTO. The next step was to extract the PBNO-NR by etching out the AAO template. Thus obtained PBNO-NR attached on FTO was given treatment of Ag-sol over the external surface of vertically aligned nanorod array.

The crystal structure of the materials determined by the X-ray diffraction (Mac Science Co., M18XHF) analysis using Cu K_α radiation at 40 kV and 200 mA. The presence of nanocrystals over the perovskite base material was confirmed by HRTEM (Phillips Model CM 200). Morphologies of photocatalysts were investigated using a scanning electron microscope (FESEM, FEI XL30L). The bandgap energy of these materials were measured by UV-vis diffuse reflectance spectrometer (Shimadzu, UV 2401).

The photoelectrochemical measurements of the films were carried out using a standard three-electrode cell using Ag/AgCl (3 M NaCl) reference electrode with a platinum gauze as a counter electrode and potentiostat (Potentiostat/Galvanostat, EG&G 263A). An electrolyte solution of 0.1 M NaOH was used for all the electrochemical measurements. The photocurrent–potential curves were recorded using >420 nm radiation obtained by using an optical filter along with a 300 Watt Xe-lamp. In order to measure the rates of H_2 and O_2 evolution, the gas phase of the reactor was analyzed under the chronoamperometry conditions using a sealed two-electrode cell with photoelectrode (working electrode) and a platinum foil (counter electrodes) without a bias voltage.

Supporting Information

Supporting Information is available from the Wiley Online Library or from the author.

Acknowledgements

This work was supported by KBSI grant T30320 and Hydrogen Energy R&D Center, (one of the 21st Century Frontier R&D Program) and the Brain Korea 21 Project, funded by the Ministry of Education, Science, and Technology (MEST) of Korea.

Received: November 11, 2010
Revised: January 28, 2011
Published online: March 23, 2011

[1] K. Sivula, F. L. Formal, M. Gratzel, *Chem. Mater.* **2009**, *21*, 2862.
[2] M. R. Hoffman, S. T. Martin, W. Choi, D. W. Bahnemann, *Chem. Rev.* **1995**, *95*, 69.
[3] X. Zong, H. Yan, G. Wu, G. Ma, F. Wen, L. Wang, C. Li, *J. Am. Chem. Soc.*, **2008**, *130*, 7176.
[4] D. K. Zhong, J. Sun, H. Inumaru, D. R. Gamelin, *J. Am. Chem. Soc.* **2009**, *131*, 6086.
[5] C. Santato, M. Ulmann, J. Augustynski, *Adv. Mater.* **2001**, *13*, 511.
[6] F. L. Formal, M. Graetzel, K. Sivula, *Adv. Funct. Mater.* **2010**, *20*, 1099.
[7] K. Maeda, K. Teramura, D. Lu, T. Takata, N. Saito, Y. Inoue, K. Domen, *Nature* **2006**, *440*, 295.
[8] R. Wang, K. Hashimoto, A. Fujishima, M. Chikuni, E. Kojima, A. Kitamuram, M. Shimohigoshi, T. Watanabe, *Nature* **1997**, *388*, 431.
[9] J. Yu, A. Kudo, *Adv. Funct. Mater.* **2006**, *16*, 2163.
[10] H. G. Kim, D. W. Hwang, J. S. Lee, *J. Am. Chem. Soc.* **2004**, *126*, 8912.
[11] H. Liu, R. Nakamura, Y. Nakato, *ChemPhysChem* **2005**, *6*, 2499.
[12] M. Liu, W. You, Z. Lei, G. Zhou, J. Yang, G. Wu, G. Ma, G. Luan, T. Takata, M. Hara, K. Domen, C. Li, *Chem. Commun.* **2004**, 2192.
[13] J. Tang, Z. Zou, J. Ye, *J. Phys. Chem. B* **2003**, *107*, 14265.
[14] K. Maeda, M. Higashi, D. Lu, R. Abe, K. Domen, *J. Am. Chem. Soc.* **2010**, *132*, 5858.
[15] H. G. Kim, P. H. Borse, W. Choi, J. S. Lee, *Angew. Chem. Int. Ed.* **2005**, *44*, 4585.
[16] H. G. Kim, P. H. Borse, J. S. Jang, E. D. Jeong, O. Jung, Y. J. Suh, J. S. Lee, *Chem. Commun.* **2009**, *39*, 5889.
[17] K. Maeda, A. Xiong, T. Yoshinaga, T. Ikeda, N. Sakamoto, T. Hisatomi, M. Takashima, D. Lu, M. Kanehara, T. Setoyama, T. Teranishi, K. Domen, *Angew. Chem. Int. Ed.* **2010**, *49*, 4096.
[18] H. G. Kim, E. D. Jeong, P. H. Borse, S. Jeon, K. Yong, J. S. Lee, W. Li, S. H. Oh, *Appl. Phys. Lett.* **2006**, *89*, 064103.
[19] K. Sivula, F. L. Formal, M. Gratzel, *Chem. Mater.* **2009**, *21*, 2862.
[20] T. Abe, K. Nagai, S. Kabutomori, M. Kaneko, A. Tajiri, T. Norimatsu, *Angew. Chem. Int. Ed.* **2006**, *45*, 2778.
[21] M. Law, L. E. Greene, J. C. Johnson, R. Saykally, P. Yang, *Nat. Mater.* **2005**, *4*, 455.